6 GEOTECHNICAL EFFECTS ON SOUTH ISLAND BRIDGES AND INFRASTRUCTURE

The transportation network in the northeast part of the South Island was significantly affected by ground shaking and ground deformation due to the Kaikoura event. The Hurunui, Marlborough, and Kaikoura council districts are located in this affected zone and were the focus of post-earthquake reconnaissance efforts. There are 268 state highway bridge structures (primarily reinforced concrete) and 636 local road bridge structures within these three districts (Palermo et al., 2017). Many of these were only minimally affected by the earthquake or not affected at all, however, moderate to significant damage was observed. The key bridges of interest within each district are discussed in detail in subsequent sections.

6.1 Hurunui District

Reconnaissance efforts in the Hurunui District of North Canterbury were primarily centred around Waiau and the surrounding towns, bridges, and roads. Figure 6.1 shows an overview of the surveyed area in the Hurunui District, indicating the bridges and other infrastructure sites that were visited. A total of 15 bridges were surveyed in this district, including 10 highway bridges and 5 rural road bridges. Of these, 6 were found to have no damage or only minor indications of damage. These sites are indicated using green markers in Figure 6.1. The observations made at key sites in this district are summarised individually below.

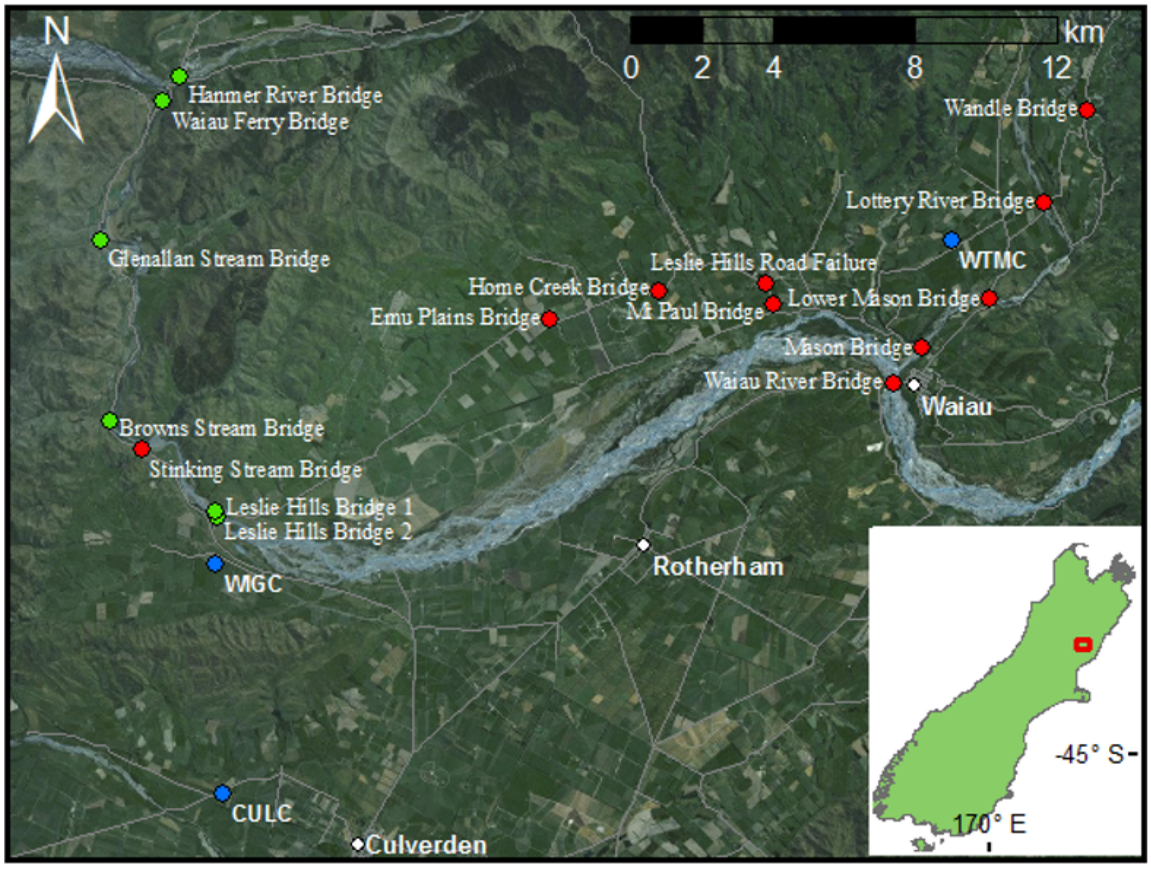

Figure 6.1: Bridge sites surveyed in the Hurunui District. Green markers indicate bridges with minor or no damage observations. Red markers indicate sites with moderate to severe damage observations. Blue markers indicate strong motion stations.

6.1.1 Waiau River Bridge [-42.6555, 173.0334]

The Waiau River Bridge is a simply-supported, precast reinforced concrete beam bridge built in 1965. The superstructure of the bridge is comprised of 33 spans with five I-beams across each of the 17 m long spans. The superstructure is supported by seat abutments and 32 wall piers. The piers are typically 4 m wide, but 7.25 m wide at the passing bays. The deck sits on 12-mm thick neoprene strip bearings at each support and is transversely restrained by dowels that secure the end diaphragms of the deck at the piers and abutments (Palermo et al., 2017). The overall structural damage to the Waiau River Bridge was moderate, and the bridge was passable with speed restrictions during the survey period of 17-18 November 2016. Gravel fill was added to the approaches on both ends of the bridge to account for the settlement and allow vehicles to smoothly pass over the bridge.

Figure 6.2 shows a general layout of the western approach to the Waiau Bridge. The abutment is located where the green polygon is placed, and the bridge deck is elevated over the river bank for about 100 m before encountering the river proper. The river was running higher than depicted in the photo, but the edge of the water was in about the same location. Clear evidence of liquefaction and lateral spreading was observed at this site, with corresponding damage to the approach embankment and bridge abutment. There was settlement of the approach embankment relative to the bridge deck, and there were cracks parallel to the roadway in the embankment crest and along sides of the road as shown in Figure 6.3 and Figure 6.4. The lateral cracks were approximately 4-5 cm wide and up to 10-12 cm wide in places. It is likely that the gravel spread over the roadway obscured further cracking and the damage in the embankment.

Figure 6.2: Site layout for western approach to Waiau River Bridge [-42.65555, 173.0302].

The magnitude of the settlement and outward movement at the western abutment was indicated by the relative movement of the various structural members. As shown in Figure 6.4(b), a concrete wingwall on the south side of the abutment (with the person standing on it) moved outwards by 10-20 cm and settled relative to the abutment wall by about 40-50 cm (pre-earthquake photos indicate that all of the concrete bodies on this side of the approach were originally flush and level). The outward movement was greater further away from the abutment (i.e., 10 cm at the abutment wall, 20 cm further back). Similar settlement of 40-50 cm was observed at the abutment wall on the north side (not shown here). The construction detailing is different on the north side, so there was not a direct way to measure the outward movement, but the outward deformation appeared to be similar in magnitude.

Figure 6.3: Lateral cracking on road side in western approach embankment of Waiau River Bridge. Photos taken looking east towards bridge [-42.6556, 173.0294]: (a) North side; (b) South side.

Figure 6.4: South side of western approach embankment to Waiau River Bridge [-42.6556, 173.03]: (a) Lateral cracks in embankment side; (b) Settlement and outward movement at abutment wall.

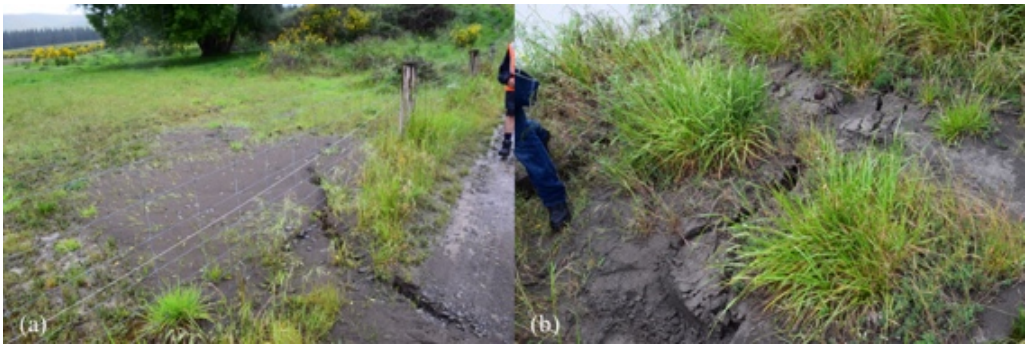

Figure 6.5: Surficial evidence of liquefaction at western approach to Waiau River Bridge: (a) Ejecta and cracking adjacent to southern toe of approach embankment [-42.6558, 173.0297]; (b) Lateral spreading cracks near river bank [-42.6556, 173.0312].

Sediment ejecta were observed on the near the toe of the southern side of the embankment (in the approximate vicinity of the blue polygon shown in Figure 6.2). The ejected material was spread over an approximately 5 m diameter area as shown in Figure 6.5(a). The particle size distribution for this ejecta material (as well as samples recovered from other bridge sites in the Hurunui district) is provided in Figure 6.6. Lateral spreading cracks parallel to river were also observed closer to the river bank, with a representative example shown in Figure 6.5(b). Ejected material was also observed in the vicinity of these cracks, but with a lesser volume of material than was found at the toe of the approach embankment. The observed lateral spreading cracks were relatively minor, with widths typically less than 5 cm. The cumulative deformation of the river bank indicated by the cracks was also relatively minor, on the order of 20-30 cm.

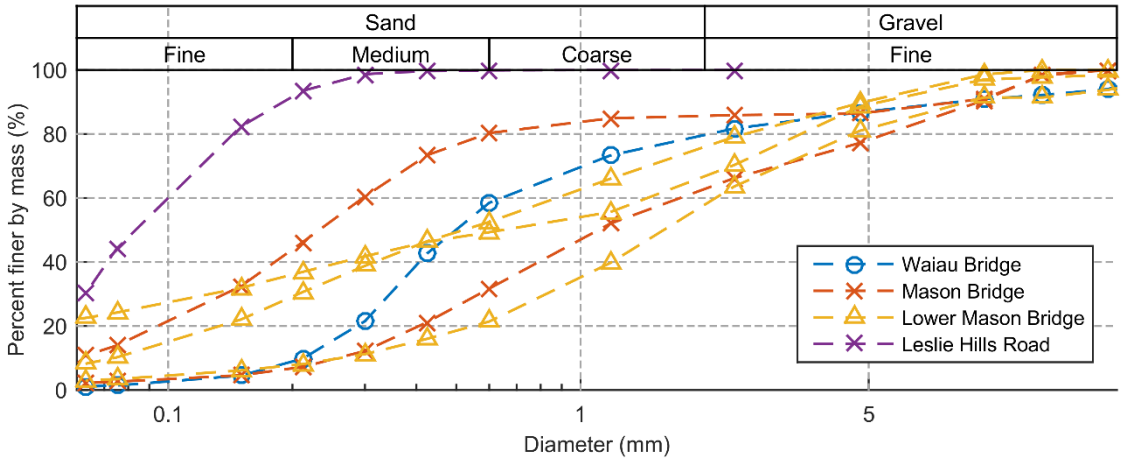

Figure 6.6: Particle size distributions of ejecta samples recovered at bridge sties in the Hurunui district

Structural damage indicative of liquefaction and lateral soil deformation was also observed. The riverward face of the western abutment wall had significant cracks and had potentially undergone some back rotation (i.e., lower portion moved closer to river than top portion). The cracking is indicated in Figure 6.7(a), where it appears that a chunk of the concrete has completely broken free from the main body of the wall. The soil subsidence on the abutment side is also visible in Figure 6.7(a) as the difference between the current ground surface and the markings on the abutment wall and through the exposure of the underside of the abutment.

Further deformation was observed at the bridge piers, most significantly in the form of differential settlement and twisting of the second pier from the western abutment, resulting in the rotation of the bridge deck shown in Figure 6.7(b). The settlement was larger on the north side of the pier, resulting in the dip in the roadway shown in Figure 6.7(b). The evidence of twisting was further indicated by the expansion gap in the bridge deck above this pier, which had widened on the south side, and had been compressed on the north side. This settlement may be liquefaction-related, but no ejected material was observed near the second pier. Most of the bridge piers showed cracks at the interface with the pile caps with some minor spalling of cover concrete, with a representative example shown in Figure 6.8(a). At some of the piers near the waterway, this damage mode was more severe, with longitudinal bar exposure and buckling as shown in Figure 6.8(b). It is likely that this damage at the base of the wall piers is due primarily to inertial loads during strong shaking.

Figure 6.7: Structural damage at western approach area to Waiau River Bridge [-42.6556, 173.0302]: (a) Severe cracking in the abutment wall (looking west from under the bridge deck); (b) Differential settlement at second pier (looking east).

Figure 6.8: Structural damage to base of piers for Waiau River Bridge [-42.6553, 173.0351]: (a) Cracking at pile cap interface; (b) Exposure and buckling of longitudinal bars.

The surveyed area and some features of interest at the eastern approach of the Waiau Bridge are shown in Figure 6.9. The damage at this approach was nominally similar to that observed at the western side. There was clear evidence of liquefaction and lateral spreading, as well as lateral cracking, settlement, and outward deformation of the approach embankment relative to the abutment wall. As with the western approach, gravel was added to the roadway to accommodate the settlement of the approach.

Figure 6.9: Site layout eastern approach to Waiau River Bridge [-42.6552, 173.037].

Representative photos of the liquefaction ejecta observed near the eastern approach are shown in Figure 6.10. There were various smaller sand boils, such as that shown in Figure 6.10(a), in the paddock north of the bridge (gold polygon in Figure 6.9). Samples could not be obtained without jumping a fence and entering the paddock, but the ejected material appeared to be visually similar to the material collected on the western side. Lateral spreading cracks were also observed on the eastern river bank, with some representative examples shown in Figure 6.11. As shown, the cracks are relatively minor. Based on observations from the bridge deck, it is possible that some of the piers have moved slightly, the cracked area could not be accessed to obtain a direct measurement. A cumulative deformation of perhaps 20 cm across the river bank was indicated by the cracks based on the deck-based survey.

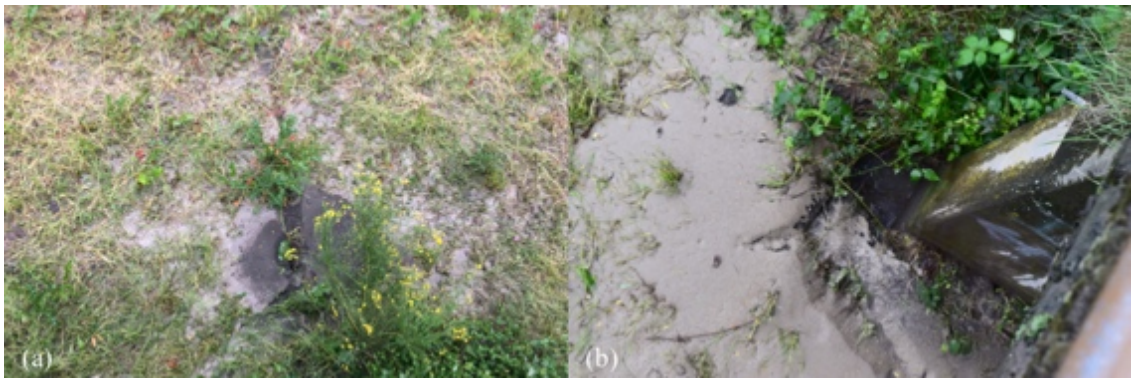

Figure 6.10: Liquefaction ejecta near the eastern approach to Waiau River Bridge [-42.6552, 173.037]: (a) Ejecta in paddock on north side of bridge; (b) Ejecta directly adjacent to bridge pier on south side.

Figure 6.11: Lateral spreading cracks with ejecta near the eastern approach to Waiau River Bridge [-42.65525, 173.036].

Figure 6.12: Lateral cracking on both sides of roadway in eastern approach embankment to Waiau River Bridge [-42.6551, 173.0380]: (a) Northern side (looking east away from bridge); (b) Southern side (looking east).

Figure 6.13: Settlement and outward movement at north side of eastern abutment to Waiau River Bridge as indicated by offset of concrete members [-42.6552, 173.037].

Representative photos of the cracks parallel to the roadway observed in the eastern approach embankment are shown in Figure 6.12 These cracks essentially extend over the full 40-50 m length of the embankment and are up to 10 cm wide. There were additional lateral cracks on the outside of the guard rails of similar scope, as well as a few minor 1-2 cm wide cracks in the roadway itself (not shown here).

As with the western side, the settlement and outward movement of the eastern approach embankment relative to the abutment wall is well indicated by the relative movement of structural members as shown in Figure 6.13. The settlement on the northern side (that shown in Figure 6.13) was 18-20 cm, with larger settlement with increasing distance from the centre of the road. The relative lateral movement of the concrete members shown indicates 10 cm of outward deformation in the approach. The settlement and outward movement on the south side of the road were similar in form to that shown for the north side, but slightly lesser in magnitude, with about 14-16 cm of settlement and 5-6 cm of outward movement indicated by the relative movement of the various concrete members. The outward movement of the embankment is greater further back from the abutment, as the lateral cracks in the embankment (e.g., Figure 6.12) indicate at least 20 cm of outward deformation. Unlike the western side, no significant damage was observed in the eastern abutment wall; however, evidence of subsidence in the fill in front of the abutment was observed, with some pile exposure below the abutment wall.

6.1.2 Mason Bridge [-42.6469, 173.0431]

The Mason Bridge is a 197 m long, 3.73 m wide reinforced concrete bridge built in the 1980s to span the Mason River on River Road. The deck is supported on 16-18 m long precast double hollow core units supported on single column bents with hammerhead pier caps over 12 spans. The lateral load resisting system at this bridge consists of transverse shear keys at the abutments and internal shear keys at all of the piers (Palermo et al., 2017). Figure 6.14 shows a general layout of the surveyed site at the Mason Bridge, indicating the locations of some of the geotechnical features of interest described in the following discussion.

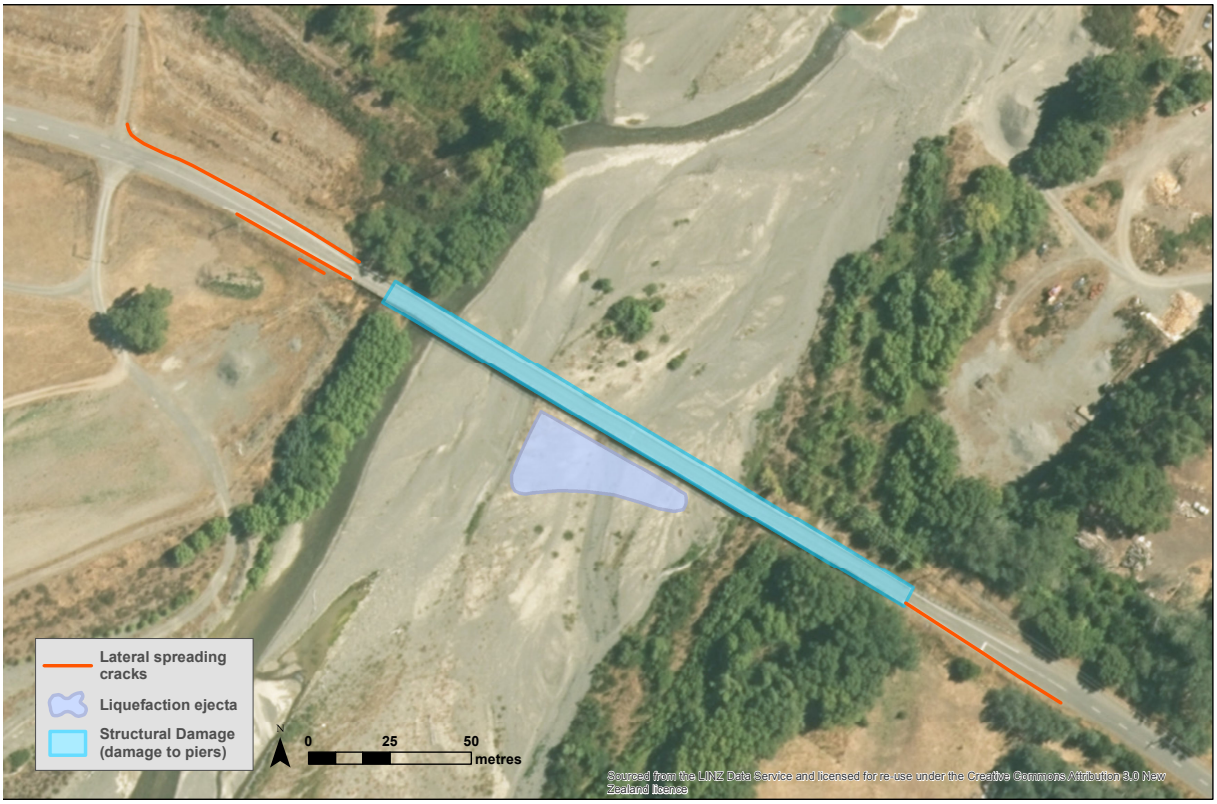

Figure 6.14: Surveyed area and features of interest for Mason Bridge [-42.6469, 173.0431].

Cracks were present in the western approach embankment parallel to roadway as shown in Figure 6.15, indicating outward spreading of the embankment. The cracks were about 5-10 cm wide and there were more on the southern side than on the northern side. No surficial evidence of liquefaction was observed near the western approach, and it is not clear if this damage is liquefaction-related. The settlement and relative movement at the western abutment was minor, with evidence suggesting a maximum of 2 cm of relative movement between the abutment and deck. No cracks or ground deformation occurred in the fill in front of the abutment as would be expected for significant abutment movement.

Figure 6.15: Cracks along edges of the western approach embankment for Mason Bridge (looking east towards bridge) [-42.6464, 173.04196]: (a) North side; (b) South side – inset shows close-up of cracks as indicated.

The southern edge of the roadway on the eastern approach to the Mason Bridge was cracked parallel to the road axis. Smaller cracks were observed on the northern side of the eastern approach, with a representative example shown in Figure 6.16(b). A power pole located at the crest of a second embankment directly adjacent to the approach is askew and has clearly moved towards the bridge and towards the river as shown in Figure 6.16(a). The power lines were pulled out of alignment, and there was more movement at the base of the pole than at the top (back rotation). The settlement of the embankment at the abutment wall was very minor, and only minor cracks were apparent in the approach roadway. No evidence of surficial liquefaction was visible on either side of the eastern approach embankment, though ejected material was found on the eastern river banks near the approach.

All of the piers for the Mason Bridge had significant damage at the connection to the footings, indicative of plastic hinging during shaking. Figure 6.17 shows some of the worst examples. In some cases, only the cover concrete was involved, while in others, the spiral reinforcement was exposed. On the piers shown in Figure 6.17, the longitudinal reinforcement is exposed and has buckled. The significance of the plastic hinging damage increased towards the centre of the bridge. Near the abutments, the spalling was concentrated towards the longitudinal direction. Near the centre, the spalling damage was concentrated on the on the southern side of the piers, indicative of strong shaking perpendicular to the main axis of the bridge. It is not clear if the piers have undergone permanent deformation due to soil failure, as only small (2-3 cm) gaps were observed between some of the footings and surrounding soil.

Figure 6.16: Northern side of eastern approach to Mason Bridge (looking west) [-42.6475, 173.04465]: (a) Power pole has moved down the slope of an embankment directly adjacent to bridge approach embankment; (b) Cracks parallel to roadway in embankment fill.

Figure 6.17: Severe examples of plastic hinging at base of Mason Bridge piers (looking north) [-42.6469, 173.0432].

Figure 6.18: Ejecta near bridge piers and footings at Mason Bridge [-42.647, 173.043]: (a) Looking east; (b) Looking north; (c) Looking west; (d) Looking north.

Liquefaction ejecta was present at nearly all of the piers on the eastern river bank, with larger volumes of ejected material for the piers closer to the river. Some characteristic examples are shown in Figure 6.18. A sample was obtained from the ejecta surrounding the fourth pier from the western abutment, and the particle size distribution is presented in Figure 6.6. Ejecta was also prevalent all over the eastern river bank, with particularly large volumes of ejected material where there was no vegetation and smaller volumes in the grassy areas. The ejecta typically had a tan-brownish film of silty fines on top, then a greyish coarser sand below this, grading coarser with depth. The ejecta on the river bank was quite weathered by the survey date of 17-18 November 2016.

6.1.3 Lower Mason Bridge [-42.6343, 173.0664]

The Lower Mason Bridge is a single-lane, 8-span reinforced concrete bridge, supported by 7 single-column piers located on Inland Road north of Waiau. The general layout of this bridge site is shown in Figure 6.19. The bridge is about 165 m long from abutment to abutment (each span is 20.7 m long based on measurements taken on the deck). The deck is supported by two 150 cm tall concrete I-girders that sit about 3 m apart centre-to-centre. The bridge girders are simply-supported and seated on elastomeric bearing pads at both abutments and at all internal piers. Transverse shear keys are present at all piers excepting the central pier, however, there is a gap built-in between the deck girders and the shear keys such that there is a degree of seismic isolation for transverse shaking (Palermo et al., 2017). No shear keys are present at the abutments. Expansion joints are located at the centre of the bridge and at either abutment, and the embankment slopes on all four sides were roughly 2:1 (horizontal to vertical).

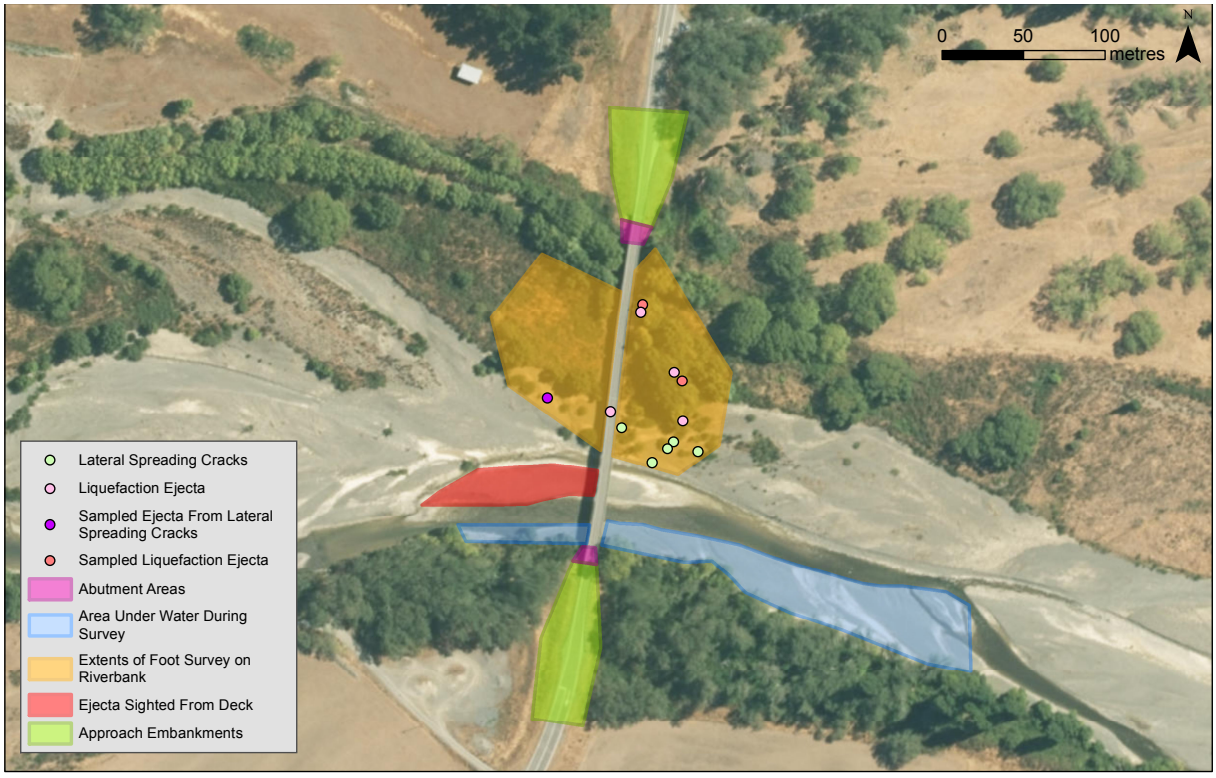

Figure 6.19: Overview of Lower Mason Bridge site indicating areas surveyed and some key features of interest [-42.6343, 173.0664].

Cracking, settlement, and outward movement (i.e. away from longitudinal bridge axis) were observed in both the southern and northern approach embankments. Some representative cracking on the roadway is shown in Figure 6.20, and some representative cracking on the embankment sides is shown in Figure 6.21. The cracks in the roadway were concentrated at the edges of the pavement, but there were a few more centrally located as well as a few sporadic transverse cracks oriented perpendicular to the axis of the road. The cracks in the roadway were generally fairly narrow in width, with most about 3-4 cm wide, but there were areas with cracks up to 30 cm wide.

Figure 6.20: Cracking in approach roadways at Lower Mason Bridge: (a) Western side of south approach looking north [-42.6353, 173.0662]; (b) Eastern side of south approach looking north [-42.6353, 173.0662]; (c) North approach looking northwest across road [-42.6330, 173.0666].

At the southern approach, the cracks adjacent to the roadway extended back about 41 m from the abutment on the east side and 28 m on the west side. At the northern approach, the lateral cracking on the road side extended back about 33 m and 20 m on the west and east sides, respectively. There may have been more cracks in the centre of the roadway, but the gravel

placed on the roadway for both approaches to accommodate the settlement likely obscured some deformation features. The gravel on the south approach extended back about 73 m from the abutment, though not over the full width of the road past about 30 m. On the north side, the gravel extended back about 15 m from the abutment wall over the full width of the road.

Figure 6.21: Cracking in sides of approach embankments at Lower Mason Bridge. (a) West side of south approach looking north [-42.6353, 173.0662]; (b) East side of south approach looking north [-42.6353, 173.0662]; (c) and (d) West side of north approach looking north and south, respectively [-42.6330, 173.0666].

The cracks in the sides of the embankments generally extended over lesser lengths than those in the roadway, and were more severe on the western sides of both approach embankments. The cracks in the western side of the southern approach embankment were about 26 m long, extending back from the outside corner of the abutment wall, and up to 30 cm wide. On the western side of the northern approach embankment, the zone of cracking was not one continuous crack, but instead a series of discrete cracks. These were about 5 cm in width, and individually about 5 m long. On the east side of the northern approach, some rip-rap material had evidently moved out perpendicular to the road axis by at least 10 cm. The cracks in at the edge of the roadway and in the sides of the embankments indicate up to about 40 cm of cumulative outward deformation of the embankment fill in both directions.

The guard rails and posts in both approach embankments were damaged as indicated in Figure 6.20(c), This damage was most likely primarily due to shaking, and the damage at the northern approach was more severe than at the southern approach. The posts have been pulled out of the ground and sheared in pieces in some places, and cracks in the soil propagate out way from most of the posts.

Figure 6.22: Settlement and outward movement at west side of north abutment to Lower Mason Bridge [-42.6334, 173.0666]: (a) Edge of abutment wall looking east; (b) Abutment wall looking north; (c) Edge of abutment wall looking north; (d) Embankment side of abutment wall near deck connection looking south.

The settlement and outward deformation of the embankment soils was clearly evident at the abutment walls, as there were marks on the abutment walls indicating the original position of the soil as shown in Figure 6.22. Though the western side of the northern abutment is shown here, the photos are typical of all four sides; however, a trench for a replacement water line dug at the western side of the southern approach embankment obscured the position of the settled native soils. Settlements on the bridge side of the abutment walls were on the order of 50-60 cm at both abutments. On the approach side of the north abutment (see Figure 6.22(d)), the settlements are approximately 35 cm, though there is newly-placed gravel fill obscuring the full extents of the settlement here. The outward bulging of the soil at the abutments was approximately 10-15 cm on the three sides where it could be measured (all except western side of the south abutment where utilities work erased evidence), with a typical example shown in Figure 6.22(c). This is less than is suggested by the cracks in the roadway and embankment sides, but not excessively.

Figure 6.23: Cracking and gapping in fill below bridge deck at northern abutment to Lower Mason Bridge indicating riverward movement of the fill [-42.6334, 173.0666]: (a) Looking north; (b) 60 cm gap between wall and fill.

Figure 6.24: Damage to abutment-deck connection at Lower Mason Bridge due to relative movement of abutment wall and deck. The breakaway member to the left was pushed back away from the deck and rotated 180° such that the connection point for the expansion joint faces away from the deck [-42.6334, 173.0666].

The soil and fill on the bridge side of the abutments (beneath the bridge deck) also display damage indicators consistent with riverward movement. Figure 6.23 shows some representative cracking in this fill material as well as the approximately 60 cm gap that has been formed by the fill soils moving away from the abutment wall. The cracks in this area on both sides of the bridge were up to 20 cm in width, and indicated a cumulative deformation of at least 1 m. It was also evident that the rip-rap (visible in the lower left corner of Figure 6.23) had undergone riverward deformation at both abutments. There were newly exposed areas where rocks had moved away from each other or from the soil. It is unclear whether or not this movement is due solely to shaking, due solely to lateral spreading, or to some combination of the two.

Some of the structural damage at the bridge is further indicative of the deformations that have occurred at the site. Figure 6.24 shows the northern abutment-to-deck connection. The breakaway concrete member indicated has been pushed back away from the bridge and flipped over such that the metal and rubber material that formed the expansion joint is now on the abutment side. This type of damage to the breakaway member was found at both abutments, and in both cases the distance between the abutment wall and deck was less than as designed. Further evidence of the riverward movement of the abutments at each side is found by the buckled guard rails at the central expansion joint connecting the two main spans of the bridge as shown in Figure 6.25. It is likely that shaking-related deformation accounts for some of this, but the deck spans are at least 10 cm closer together than normal at the centre of the bridge.

Figure 6.25: Buckling of guard rails at centre expansion joint of Lower Mason Bridge indicating that the two main deck sections have undergone permanent inward deformation. Photo facing south [-42.6343, 173.0664].

Figure 6.26: Cracks in northern river bank on eastern side of bridge. Photo taken from bridge deck. Riverward direction is down for this orientation [-42.6342, 173.0665].

Liquefaction ejecta and lateral spreading cracks were observed throughout the northern river bank area near the bridge as indicated in Figure 6.19. These features were observed both from the bridge deck and via a foot survey of the riverbank area. Figure 6.26 shows some of the

lateral spreading cracks visible on the eastern side of the bridge, and Figure 6.27 shows some of liquefaction ejecta visible from the bridge deck located in some small islands in the middle of the main flow of the river. The remaining evidence of liquefaction and lateral spreading was only visible when down on the northern river bank around and below the bridge. Some representative examples of the cracking and sediment ejecta found in this area are shown in Figure 6.28, while particle size distributions are shown in Figure 6.6. The sediment ejecta features are mostly less than 1 m in diameter, though there are some larger more spread out areas of ejecta. Based on the lateral spreading cracks observed, the magnitude of cumulative deformation in the soil was at least 50-80 cm.

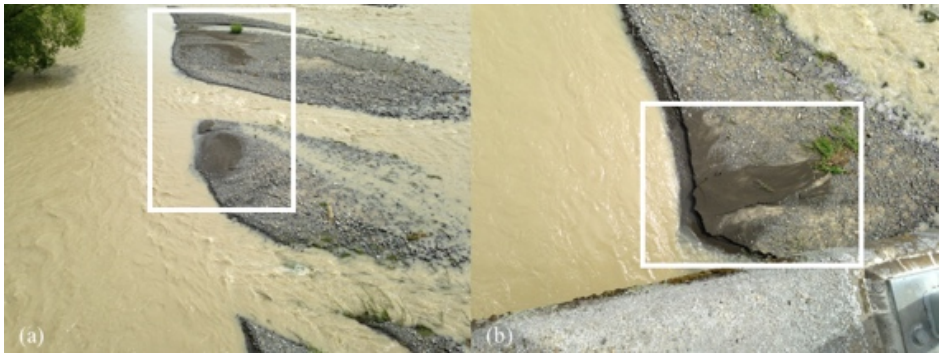

Figure 6.27: Liquefaction ejecta on west side of bridge (looking west). [-42.6345, 173.0657].

Figure 6.28: Representative photos of the lateral spreading cracking and liquefaction ejecta observed on the Northern river bank near the bridge in the areas indicated by Figure 6.19.

In addition to the permanent deformation of the bridge embankments, abutment walls, and bridge decks likely due to the evident liquefaction and lateral spreading at this site, the structural damage of Figure 6.29 indicates that shaking-related damage was a major factor in the response of this bridge. Damage consistent with plastic hinge formation was observed at

the base of all the bridge piers aside from the central pier; some typical examples are shown in Figure 6.29(a) and (b). These hinge zones displayed extensive cover spalling and a significant number of buckled and fractured bars. Further shaking damage is shown in Figure 6.29(c) and (d), with a closer view of the guardrail buckling at mid-span. The girders have also become unseated from the bearing pads at both abutments. Figure 6.29(d) shows this at the western side of the south abutment. On the eastern side of the south abutment, the girder is still atop the bearing pad, but only half of the pad is below the girder. At the north abutment (not shown here), the eastern girder is unseated and the bearing pad for the western girder is askew.

Figure 6.29: Structural damage at Lower Mason Bridge [-42.6343, 173.0664]. (a) Damage at base of piers looking south; (b) Base of southern-most pier looking north; (c) Deformation at central expansion joint looking southeast; (d) Girder unseated from bearing pad.

6.1.4 Wandle Bridge [-42.5864, 173.1003]

Wandle Bridge is a 35 m long, 3 span, precast concrete bridge spanning a portion of the Mason River on Inland Road. The Wandle Bridge had to be closed due to the severe structural damage shown in Figure 6.30, and a bailey bridge was put in place to allow vehicles to cross the river. Significant plastic hinging occurred at the base of the bridge piers, which are no longer standing vertically, significant diaphragm damage occurred in the bridge deck, and the bridge is only marginally stable. This structural damage is almost certainly shaking-related and the spalling associated with the hinging is located on the eastern side of the piers. The

geotechnical damage at this site was minor. A series of cracks were observed near the river adjacent to the toe of the southern approach embankment. These cracks are only a few centimetres wide. No surficial evidence of liquefaction was observed.

Figure 6.30: Structural damage to Wandle Bridge [-42.5864, 173.1003]: (a) South approach from under bridge; (b) Plastic hinging on pier near south approach; (c) Deck at southern end; (d) South abutment; (e) North approach from under bridge; (f) Minor hinging on pier near north abutment.

6.1.5 Lottery River Bridge [-42.6097, 173.0854]

The Lottery River Bridge is a single-lane, 6-span reinforced concrete bridge supported by single-column piers located on Inland Road about 3.5 km north from the Lower Mason Bridge. The structural design of this bridge is nominally identical to the Lower Mason Bridge, just adapted for a shorter overall span (Palermo et al., 2017). Figure 6.31(a) shows the transverse shear key at one of the interior piers and the lack of a shear key at the central pier. The observed structural damage at the Lottery River Bridge was similar in nature to the

Lower Mason Bridge, with compression failure of the expansion joint over the central pier, residual displacements and unseating over some of the elastomeric bearing pads, and uneven residual spacing of the expansion joints. The base of the piers at the Lottery River Bridge also displayed damage consistent with full plastic hinge formation, with a typical example shown in Figure 6.31(b).

Figure 6.31: Lottery River Bridge [-42.6097, 173.0854]: (a) General layout; (b) Plastic hinge damage at base of pier.

Settlement and transverse deformation of the approaches was observed at both abutments, with a similar scope to that detailed for the Lower Mason Bridge. Approximately 40 cm of settlement was observed in the fill ahead of both abutments. Figure 6.32(a) shows the northeast approach, but any cracks are obscured by the gravel fill used to accommodate the settlement. There was residual relative displacement between the deck and abutments on both sides of the bridge, with the deck moving north relative to the abutments on both sides. Figure 6.32(b) shows the residual transverse displacement at the northeast side, and Figure 6.32(c) shows the residual longitudinal displacement at the southwest abutment, as well as the residual movement of the bearing pad for this beam.

Figure 6.32: Damage at Lottery River Bridge [-42.6097, 173.0854]: (a) Gravel in-fill due to settlement and guardrail damage at northeast approach looking northeast; (b) Residual transverse offset of deck and abutment at northeast abutment looking southwest; (c) Residual displacement of bearing pad at southwest abutment looking west.

6.1.6 Stinking Stream Bridge [-42.6724, 172.7748]

Visual surveys along Highway 7 between Culverden and the turn-off for Hanmer Springs indicated two primary areas of interest. The locations of these sites are shown in Figure 6.33(a) with close-up site layouts provided in Figure 6.33(b) and (c). Their location relative to the wider survey area is shown in Figure 6.1. The Stinking Stream Bridge is a 12.2 m long, 7.3 m wide single-span, two-lane bridge that was surveyed by two reconnaissance teams, first on 14 November and then again on 17 November 2016.

Figure 6.33: Highway 7 area: (a) Site locations for areas of interest; (b) Road crack site layout [-42.6310, 172.7718]; (c) Stinking Stream Bridge site layout [-42.6724, 172.7748].

There were roadway settlements at the abutments of about 5-10 cm, with corresponding transverse cracks as shown in Figure 6.34. There were also longitudinal cracks in the roadway indicative of outward movement of the approach soils. The magnitude of the outward movement and settlement increased with distance away from the road centreline. At the northern corner, the settlement appeared to be about 20-40 cm as shown in Figure 6.35(d), while at the other corners the settlement is less (about 5-10 cm). Longitudinal cracking was also present in the soils adjacent to the road way at the east, north, and west corners of the bridge as shown in Figure 6.34(d), Figure 6.35(b), and Figure 6.36(d), respectively. These cracks have a maximum width of about 5 cm. The rip-rap below the abutments has moved

towards the stream and down away from the abutment, exposing the base of the abutment. This is shown for the western corner in Figure 6.36(b) and (c). No surficial evidence of liquefaction was noted at this site and no mechanism for the damage has been identified.

Figure 6.34: Stinking Stream Bridge [-42.6724, 172.7748]: (a) Looking north on 14 November; (b) Southern corner on 14 November; (c) and (d) Eastern corner on 17 November.

Figure 6.35: Northern corner of Stinking Stream Bridge [-42.6724, 172.7748]. (a) Looking south on 14 November; (b) Looking south on 17 November; (c) Hole in roadway; (d) Settlement on 17 November.

One interesting feature at the Stinking Stream Bridge is given by Figure 6.35(a) and (b), which show essentially the same view of the northern corner of the bridge on 14 and 17 November, respectively. The visual damage on 17 November is more severe than it was on the day following the main shock. The longitudinal cracking is more extensive, and an

approximately 50 cm diameter hole has opened up in the road surface. This suggests four possibilities: (1) ground deformation did not change, but pavement damage only occurred after traffic was reopened; (2) additional time-dependent ground deformation occurred; (3) additional ground deformation occurred due to aftershocks; or (4) some combination of the three possibilities.

Figure 6.36: West corner of Stinking Stream Bridge [-42.672427, 172.774764]: (a) Settlement and cracking at abutment; (b) Settlement looking east; (c) Rip-rap movement away from the abutment base; (d) Cracking in approach.

Figure 6.37: Cracks on free-face side of roadway on Highway 7 looking south [-42.6310, 172.7718]. Location and site layout shown in Figure 6.33.

The other site of note along the surveyed stretch of Highway 7 are the roadside cracks shown in Figure 6.37. The location and layout of this site are provided in Figure 6.33(a) and (b), respectively. The cracking shown in Figure 6.37 is approximately 50 m long and up to 30 cm

wide and involved the free face of a section of road that passes along a slope. The Waiau River flows off to the left of the photos shown in Figure 6.37. No evidence of liquefaction was observed near the cracks, but possible evidence of liquefaction, in the form of pooling water, was observed closer to the river bank in the general area of this ground deformation.

6.1.7 Home Creek Bridge [-42.6323, 172.9528]

Visual surveys in the Emu Plains area located northwest of Waiau Township identified a number of sites of interest along Leslie Hills and River Roads, particularly at a series of rural bridges on Leslie Hills Road. The locations of these sites are shown in Figure 6.1. Home Creek Bridge is an 8 m long, 3.67 m wide single-span and single lane precast and pre-tensioned concrete bridge spanning a section of Home Creek on Leslie Hills Rd. Visual surveys at the Home Creek Bridge site indicated 15-20 cm wide transverse roadway cracks in the western approach to the bridge. As shown in Figure 6.38(a), there were 3 or 4 of these cracks in the approach, indicating an accumulated extension towards the bridge/stream of at least 45 cm. There was about 25-30 cm of settlement at the western abutment and wingwalls as shown in Figure 6.38(b), (c), and (d). For context, the callipers resting against the abutment wall in Figure 6.38(b) are 20 cm long. There were also a few transverse cracks in the approach near the abutment, but it appears that the wingwalls held the soil back sufficiently without any notable structural damage indications.

Figure 6.38: Home Creek Bridge [-42.6323, 172.9528]: (a) Roadway cracks in western approach; (b), (c), and (d) Settlement at western abutment.

6.1.8 Leslie Hills Road Failure [-42.6306,172.9895]

As Leslie Hills Road turns southeast towards River Road (see Figure 6.1), extreme damage was encountered in the roadway. As shown in Figure 6.39, a section of road adjacent to an escarpment has completely failed, breaking up into several chunks with a total vertical offset of 1.5 to 2 m. It is likely that some portion of the failed material was man-made fill given the difference between the topography to the right of the road in Figure 6.39(a) and the former topography of the road. Evidence indicates that this road failure is related to surface faulting, however, there was also evidence of excess pore water pressure build-up or liquefaction, as some minor liquefaction ejecta was sighted nearby.

There is also significant damage to the road to the west and east of the major failure zone. Figure 6.39(c) and Figure 6.40 show some representative photos of the damage observed to the west of the major road failure, indicating some significant transverse and longitudinal cracks in the road, a somewhat smaller road failure area adjacent to a side slope, and some cracking through a paddock next to the roadway. On the east side of the major failure zone on Leslie Hills Road, the damage is characterised by compression of the roadway material as evidenced by the compression ridging shown in Figure 6.41(a) and (b). The damage to the roadway on the east side of the large failure zone is essentially continuous up to the Mt Paul Bridge discussed in the next section.

Figure 6.39: Failure and severe cracking on Leslie Hills Road (photos all taken looking west) [-42.6306,172.9895]: (a) Overview of major failure area; (b) Closer view of failure area; (c) Cracking to west of failure area.

Figure 6.40: Damage west of failure area on Leslie Hills Road (both photos taken looking west) [-42.6306,172.9895]: (a) Cracking and failure of the road on free face of embankment; (b) Adjacent cracking through paddock.

Figure 6.41: Damage observations east of Leslie Hills Road failure area [-42.6306,172.9895]: (a) Compression ridging in pavement material; (b) Side view of compression ridge; (c) Minor liquefaction ejecta.

The small sand boil on the edge of the road surface shown in Figure 6.41(c) was the only surficial evidence of liquefaction (particle size distribution shown in Figure 6.6) observed in the vicinity of the major roadway failure on Leslie Hills Rd. Despite the lack of significant evidence of liquefaction at the site, excess pore pressure build-up or liquefaction of some underlying material still seems to be a possible cause for some of the ground deformation and damage observed in this area.

6.1.9 Mt Paul Bridge [-42.6355, 172.9923]

The Mt Paul Bridge is an 18.9 m long, 4.34 m wide precast concrete bridge spanning a stream on Leslie Hills Road just a few hundred metres southeast from the major failure area discussed in the previous section. The damage at this bridge site was characterised by severe cracking in the roadway and settlement of the approaches relative to the abutments and deck. Figure 6.42 shows some indications of the roadway cracking located between the Leslie Hills Road failure site and the Mt Paul Bridge. As shown, the general cracking pattern of Figure 6.42(a) found further away from the bridge gradually becomes dominated by the wider longitudinal cracks of Figure 6.42(c) found closer on to the bridge. These longitudinal cracks are approximately 20-30 cm wide and are located all across the roadway, not just at the edges. No surficial evidence of liquefaction was observed at this site, but the ejecta sited closer to the major road failure site is only a few hundred metres away.

At the immediate bridge approaches, the damage is even more severe. As shown in Figure 6.43, the soil and rip-rap below the bridge also appears to have settled and moved towards the stream, completely exposing the underside of the bridge abutments. As shown in Figure 6.44, there is significant cracking and outward movement of the approach soils, with outward deformations on the order of 40-50 cm. There is also significant settlement of the approach roadway and approach soils relative to the deck on both sides of the bridge with magnitudes on the order of 40-50 cm. For approximate reference, the elevation of the original ground surface can be discerned by the markings on the guardrail posts.

Figure 6.42: Cracking in roadway approaching Mt Paul Bridge from the north along Leslie Hills Road [-42.6355, 172.9924].

Figure 6.43: Settlement below abutment at Mt Paul Bridge [-42.6355, 172.9923].

Figure 6.44: Settlement and cracking in approaches to Mt Paul Bridge [-42.6355, 172.9924]: (a) Southwest corner; (b) Southeast corner; (c) Northeast corner; (d) Northwest corner.

6.1.10 Emu Plains Bridge [-42.6394, 172.9149]

The Emu Plains Bridge is a 20.5 m long, 4 m wide timber bridge on Leslie Hills Road at the location indicated in Figure 6.1. The damage at this bridge site was similar to that observed at all of the other surveyed rural bridges. Figure 6.45 shows some representative photos from this site. There was significant cracking in the roadway, particularly on the east side of the bridge, where the longitudinal cracks were up to 30 cm wide and the transverse cracks were about 10 cm wide with up to 20 cm of vertical offset in places. The settlement of the eastern approach ranged from about 10-20 cm with the largest settlements on the southeast corner of the bridge as shown in Figure 6.45(b). No surficial evidence of liquefaction was observed at this site, and the mechanisms for this deformation have not been identified.

Figure 6.45: Damage at Emu Plains Bridge [-42.6394, 172.9149]: (a) Roadway damage looking west towards bridge; (b) Settlement at eastern abutment; (c) and (d) Significant cracking in roadway on eastern side of bridge (photos taken facing east away from bridge).

6.2 Marlborough district

The bridge reconnaissance in the Marlborough district was based in Blenheim. Surveys were completed within Blenheim, as well as along SH63 heading west from Blenheim into the Wairau Valley, and along SH1 heading south from Blenheim towards Kaikoura. A total of 12 bridges were surveyed in the Marlborough district as shown in Figure 6.46. The bridges on SH63 and two of the rural bridges north of Blenheim did not show any signs of earthquake damage. These sites are indicated using green markers in Figure 6.46. In contrast, earthquake-induced damage was observed at all of the surveyed bridges on SH1 south of Blenheim. The key observations made at these bridge sites are discussed individually in the following subsections. Three additional SH1 bridges south of Ward were surveyed, however these sites technically fall within the Kaikoura District and are discussed in the following section along with the rest of the Kaikoura District sites.

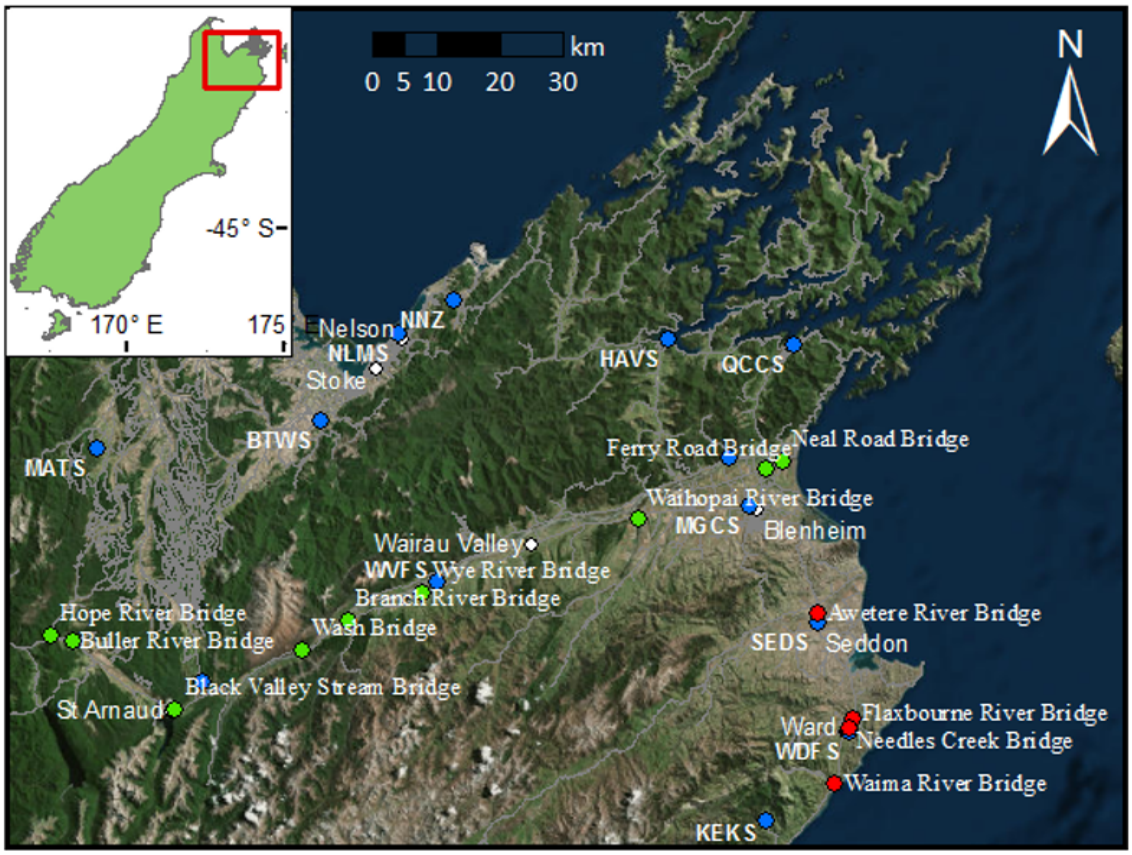

Figure 6.46: Bridge sites surveyed in the Marlborough District. Green markers indicate bridges with minor or no damage observations. Red markers indicate sites with moderate to severe damage observations. Blue markers indicate strong motion stations.

6.2.1 Flaxbourne River Bridge [-41.8085, 174.1458]

The Flaxbourne River Bridge is a 5-span reinforced concrete bridge built in the 1950s to span the Flaxbourne river north of Ward on SH1. The deck is monolithic with beams and is supported on four wall piers with abutments at either end. The superstructure is not integral to the piers, and the only lateral connection to the piers and abutments is via a series of vertical reinforcing bars working in dowel action, with two bars per beam. There are no expansion joints over the bridge span (Palermo et al., 2017).

Damage was observed in both the superstructure and substructure for the Flaxbourne River Bridge. The deck was separated from the piers and abutments, as the bars connecting the superstructure and substructure did not provide sufficient shear capacity for the lateral seismic demands. The dowel action of the bars was clearly observed, however, as the surrounding cover concrete was broken and the confining transverse reinforcement was bent and even fractured in some cases as shown in Figure 6.47(a). The severity of this damage varied along the length of the bridge, with the worst damage observed in the two southernmost piers, where the deck had been displaced southwest from the original position. The residual transverse deck displacement is shown in Figure 6.47(b) as the girder is offset from its original position. The damage to the piers themselves was more severe at the two northernmost piers where the deck-pier connection was less damaged.

Plastic hinging occurred at both abutments with exposed and buckled reinforcement, and cracking was observed at the base of some of the piers. At the southern abutment, the plastic hinging occurred at the top of the abutment columns, fully exposing the longitudinal reinforcement of the columns as shown in Figure 6.47(c). The cast-in-place soil retaining beam at this abutment had moved towards the river by approximately 200 mm and there were clear signs of longitudinal movement of the beam diaphragm atop the abutment seat as shown in Figure 6.47(d). At the northern abutment, the plastic hinging was observed at the top of the piles. Cracking was observed across the pile depth, with concrete spalling on both the front and back faces of the piles.

Figure 6.47: Damage at Flaxbourne River Bridge [-41.8085, 174.1458]: (a) Damage at deck-pier connection; (b) Residual transverse deck displacement; (c) Exposed and buckled reinforcement in abutment columns; (d) Residual longitudinal deck displacement.

An inspection of the interface between the piers and pile caps at the accessible piers (all but the southernmost pier) indicated cracking at the pier base extending through the entire interface as shown in Figure 6.48(b), (c) and (d). These piers were tilted in the longitudinal direction such that the tops of the piers had moved south, with a typical example shown in Figure 6.48(a). Exposed and buckled longitudinal reinforcing bars were observed at the northern bridge piers, and there was clear evidence of 10 mm of relative movement towards the river channel between the base of the northernmost pier and its pile cap. Moderate settlement of the approaches was observed at the Flaxbourne River Bridge with longitudinal cracking in the roadway indicative of outward spreading in the approach. No surficial evidence of liquefaction was observed at the bridge site.

Figure 6.48: Substructure damage at Flaxbourne River Bridge [-41.8085, 174.1458]: (a) Tilted pier; (b) Cracking at pier base; (c) and (d) Cracking and exposed reinforcement at base of piers.

6.2.2 Needles Creek Bridge [-41.8217, 174.1370]

The Needles Creek Bridge is a 5-span concrete bridge built in the 1950s with a structural design that is nominally identical to the Flaxbourne River Bridge. The primary difference between these two bridges is that where the Flaxbourne River Bridge is linked to the wall piers by dowels, the superstructure of the Needles Creek Bridge is integral to the piers (Palermo et al., 2017). The Needles Creek Bridge is located about 1.7 km south along SH1 from the Flaxbourne River Bridge, and is sited approximately 640 m away from the Ward fire station strong motion station (WDFS). Figure 6.49 shows an elevation view of the bridge and provides a reference numbering system for the piers and abutments. Figure 6.50 shows a plan layout of the Needles Creek Bridge site with a summary of the observed geotechnical damage and ground failures mapped in the area.

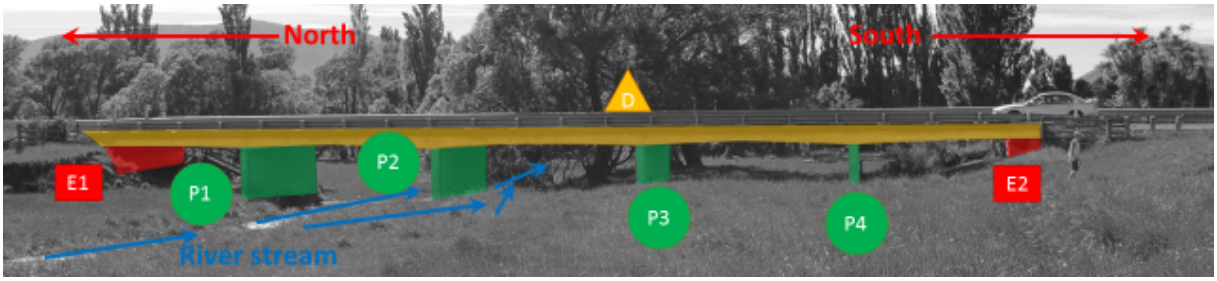

Figure 6.49: Layout of Needles Creek Bridge in elevation view.

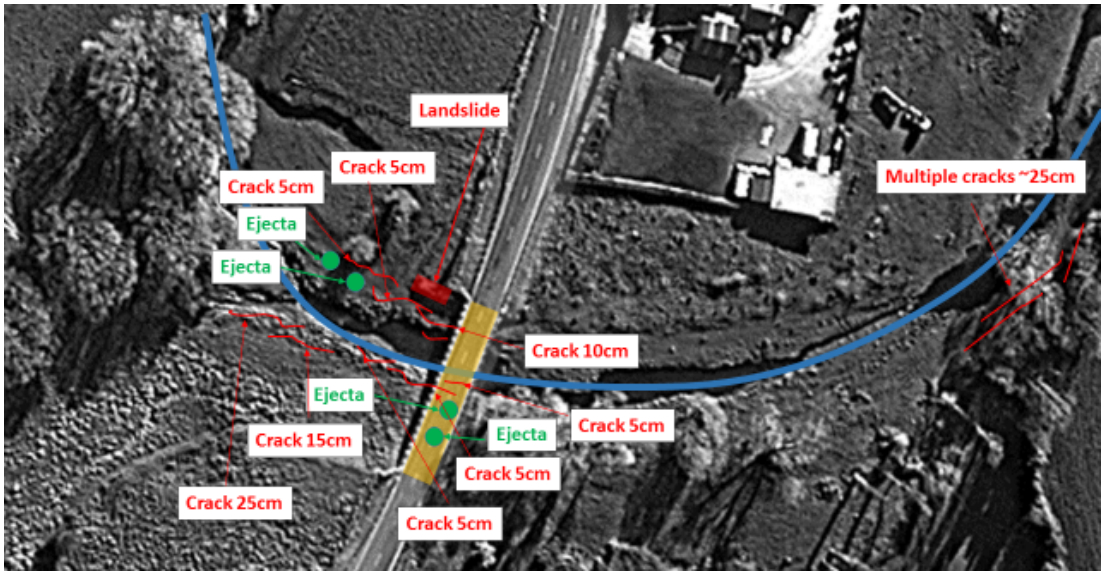

Figure 6.50: Overview of Needles Creek Bridge site with indications of ground damage. Orange area is the bridge deck, red lines indicate cracks, and the green markers indicate sand boils. The blue line indicates the creek bed.

Liquefaction ejecta was observed under the Needles Creek Bridge between piers 2 and 3 and between piers 3 and 4, as well as in the free field on the west side of the bridge as indicated in Figure 6.50. Some typical liquefaction evidence is shown in Figure 6.51. Lateral spreading cracks were also observed along the free-face of the river, extending up to the edges of the piers as shown in the site layout of Figure 6.50 and the photos of Figure 6.52. Settlement of at least 15 cm was observed at both abutment walls, completely exposing the underside of the abutments as shown in Figure 6.53. Cracks were present in nearly all of the piles visible beneath the exposed abutment bases, varying in width from 1-5 mm. Figure 6.54(a) shows a representative example of this damage. A gap of 25-30 cm was observed between the abutment piles and the surrounding soil, indicative of relative movement of the soils and foundations. Similar soil-structure gapping of 10-25 cm was observed at the base of piers 1, 3, and 4. Figure 6.54(b) shows this gapping at the base of pier 3.

Figure 6.51: Liquefaction ejecta at Needles Creek Bridge site [-41.8217, 174.1370]: (a) Ejecta between piers 1 and 2; (b) Ejecta between piers 3 and 4; (c) Ejecta in free field west of bridge.

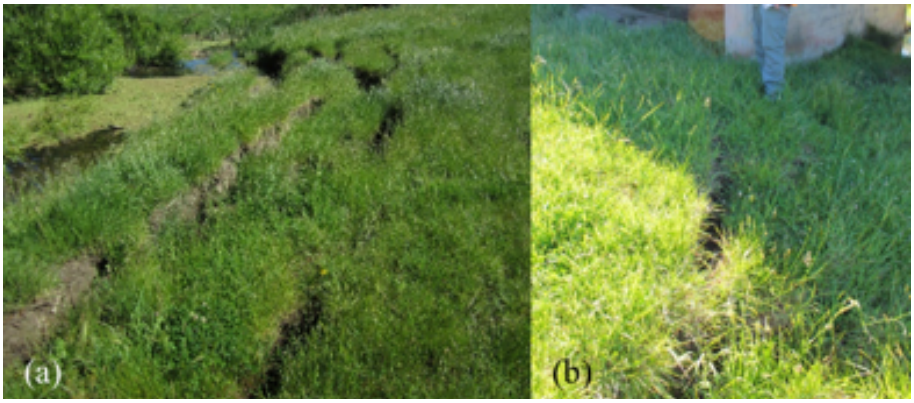

Figure 6.52: Free field lateral spreading cracks at Needles Creek Bridge site [-41.8217, 174.1370]: (a) Cracks along free face of the river; (b) Cracking near bridge pier.

Figure 6.53: Soil subsidence below abutments at Needles Creek Bridge [-41.8217, 174.1370]: (a) North abutment wall looking northwest; (b) South abutment wall looking south.

Figure 6.54: Pile and footing damage at Needles Creek Bridge [-41.8217, 174.1370]: (a) Crack in pile for south abutment; (b) Soil-footing gapping at pier 3.

Significant plastic hinging was observed at the top and bottom of the piers for the Needles Creek Bridge. As shown in Figure 6.55(a), there was a tendency for the formation of single cracks rather than distributed cracking, and for these single cracks to extend over the full width of the wall piers, which indicates that the bridge was more heavily loaded in the longitudinal direction. This inference is also supported by the observation that the bridge deck had clearly sheared off of abutment 1 on the north end as shown in Figure 6.55(b). The pier cracking was particularly severe at piers 1 and 2. Exposure and buckling of the longitudinal reinforcement was observed at the top of pier 1 as shown in Figure 6.55(c), and this pier had a measured residual tilt of about 3° from vertical as shown in Figure 6.55(d). It appeared that this tilting was due to the base of the pier moving towards the river, likely due to the lateral spreading that occurred on the banks of the creek.

Figure 6.55: Structural damage at Needles Creek Bridge [-41.8217, 174.1370]: (a) Cracking across length of pier 1 looking south; (b) Deck sheared off of abutment 1 facing west; (c) Cracking at pier 1 facing east; (d) Tilting of pier 1 facing east.

6.2.3 Waima River Bridge [-41.9021, 174.1122]

The Waima River Bridge is an 8-span bridge on SH1 constructed in 1975. The Waima River Bridge has simple spans with two precast, prestressed I-beams seated on circular monopile piers with hammerhead bents. Seismic retrofit was carried out at this bridge in 2003 to reduce the likelihood of deck unseating during earthquake shaking (Palermo et al., 2017). Figure 6.56(a) and (b) show some of the retrofitting measures. The Waima River Bridge displayed noticeable residual transverse deck displacement, with two components: a rigid body component towards the sea (eastward), and a deformation component directed primarily westward. The deformation pattern was curved between the abutments, with the largest transverse displacement at the centre of the overall bridge span. The deck was also twisted

about the longitudinal axis such that the southern edge is now higher than the northern edge. Cracking and spalling of concrete was observed around the retrofitted steel brackets attached to the deck beams, with a representative example shown in Figure 6.56(b). Cracking was also observed at both abutments and at the tops of the exposed abutment piles as shown in Figure 6.56(c). The piers near the southern abutment had a noticeable tilt with the top of the pier translated to the west. The tilt at the southernmost pier is shown in Figure 6.56(d). Minor flexural cracking was also observed around the base of some piers.

Figure 6.56: Damage at Waima River Bridge [-41.9021, 174.1122]: (a) South abutment facing south; (b) Damage to concrete beams around retrofit brackets; (c) Cracking at top of abutment pile; (d) Tilt of southernmost pier facing north.

Figure 6.57: Geotechnical damage at Waima River Bridge site [-41.9021, 174.1122]; (a) Ejecta at piers of railroad bridge 50 m upstream; (b) Settlement at south approach looking north.

Liquefaction ejecta was observed around a few of the piers of a railroad bridge running parallel to the Waima River Bridge approximately 50 m upstream as shown in Figure 6.57(a), but nothing was evident closer to the Waima Bridge itself. Settlement was observed in front of the abutment walls as shown in Figure 6.56(a), exposing the piles beneath the abutment, and approach settlement greater than 10 cm was observed at the south side of the bridge as shown in Figure 6.57(b). Relatively minor longitudinal cracks at the edge of the approach roadway were observed, indicative of a modest amount of outward spreading in the approach material.

6.2.4 Awatere River Bridge [-41.6585, 174.077]

The Awatere River Bridge is a 10-span reinforced concrete bridge constructed in 2007. The bridge superstructure consists of 1.2-m deep precast, prestressed U-beams that are integral with the piers and seated on bearings at the abutments. The deck is continuous over the length of the bridge. The interior piers consist of 5.5 m long 1.0 m diameter circular columns supported on single 1.2-m diameter steel-cased drilled shafts (Palermo et al., 2017). Flexural damage was observed in the Awatere River Bridge piers, with flexural cracking at the tops of the pier columns near the abutments, and spalling of concrete at the top and bottom of the pier columns near the middle of the bridge as shown in Figure 6.58(a) and (b). Residual displacement of the deck was evident at the southern abutment, as the bearings shown in Figure 6.58(c) indicate a residual movement in to the southeast. It is unknown if all of this residual displacement is due to the Kaikoura event or due in part to a previous seismic event such as the 2013 Lake Grassmere earthquake.

Figure 6.58: Damage at Awatere River Bridge [-41.6585, 174.077]: (a) Flexural damage at top and bottom of pier column near middle of bridge facing west; (b) Spalling of concrete at base of pier column; (c) Residual displacement in bearing pad at southern abutment; (d) Damage to previously grouted area.

It is interesting to note that all of the observed cracking and spalling had occurred in areas that had been previously repaired with grout. A typical example of this is shown in Figure 6.58(d). No surficial evidence of liquefaction was noted at the Awatere River Bridge site, and there was no significant settlement in the approaches. Settlement was observed in the fill below the bridge and in front of the abutment walls, exposing the base of the abutments, but no obvious or large transverse cracks were observed in this fill material.

6.3 Kaikoura District

Significant non-ground faulting and non-landslide damage was observed at six bridges within the Kaikoura District as shown in Figure 6.59. Three of these bridges are located on SH1 north of Kaikoura township (and north of the landslides at Okiwi Bay that are blocking access to Kaikoura from the north on SH1). Two are located just north of Oaro, a few kilometres south of Kaikoura; one is a highway bridge on SHI and the other is a railway bridge over the Oaro River. The remaining bridge is a smaller local road bridge over Lyell Creek within Kaikoura. The Clarence Valley Road Bridge (not shown in Figure 6.59), which experienced complete collapse is also briefly discussed. In addition to these larger bridges, several smaller bridges and culverts within the Kaikoura township are discussed in this section.

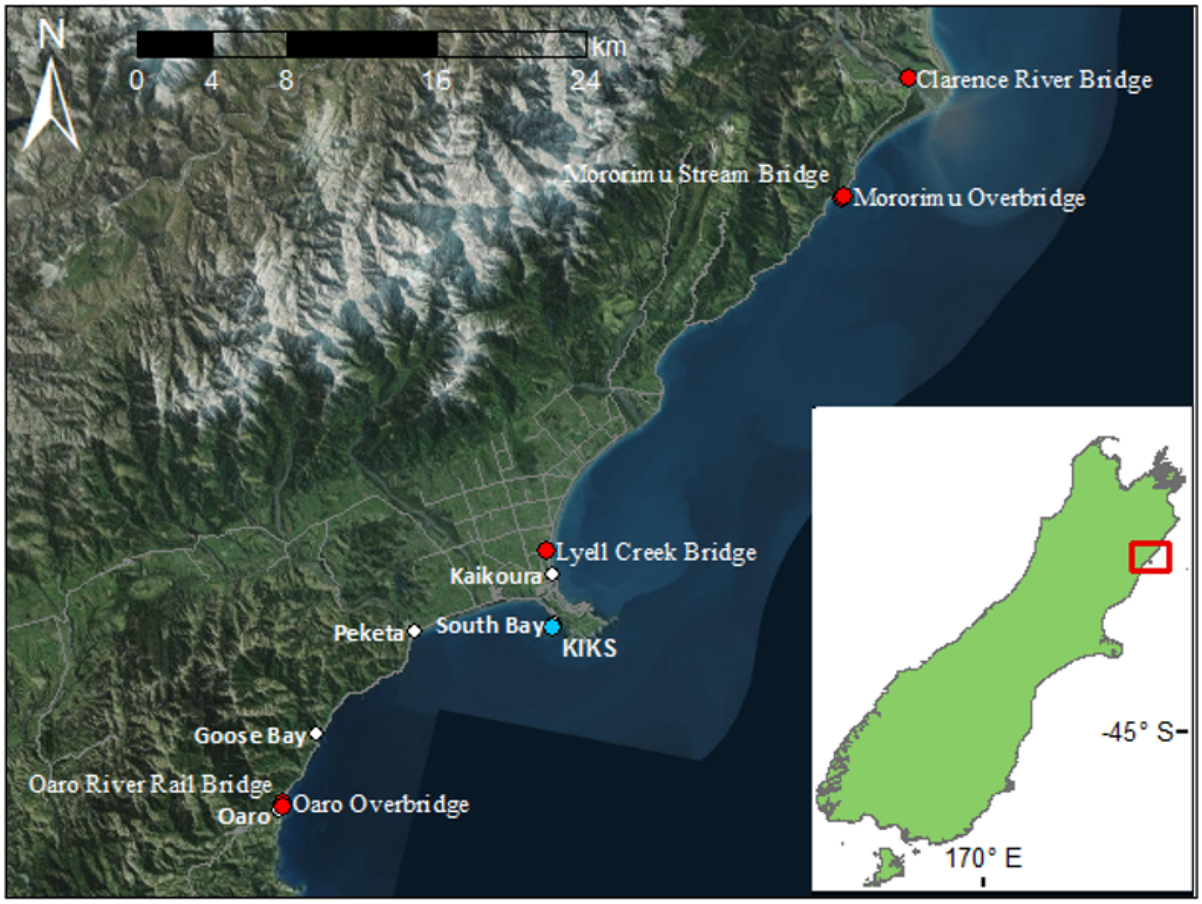

Figure 6.59: Bridge sites in the Kaikoura District with observations of moderate to severe damage. Red markers indicate bridge sites. Blue markers indicate strong motion stations.

6.3.1 Mororimu Stream Bridge [-42.2173, 173.8673]

The Mororimu Stream Bridge is a 3-span cast in-situ integral reinforced concrete structure built in 1951. The spans are supported on wall piers that are founded on strip footings. The Mororimu Stream Bridge is curved horizontally and has a vertical slope, with the north side sitting higher than the south side, and is oriented essentially directly in-line with an east-west plane (Palermo et al., 2017).

The structural damage to the bridge was primarily confined to the substructure with the exception of one minor transverse crack found in the underside of the deck near the western pier. Extensive cracking was observed in both abutments, in the abutment columns, and at the tops of the piers as shown in Figure 6.60(a)-(c). Settlement was observed in both approaches, with approximately 10 cm of settlement at the eastern abutment shown in Figure 6.60(d). Settlement and outward spreading was observed in the fill ahead of both abutments, and soil gapping of several centimetres was observed around the base of some piers. No surficial evidence of liquefaction was noted anywhere in the vicinity of the bridge site.

Figure 6.60: Damage observed at Mororimu Stream Bridge [-42.2173, 173.8673]: (a) Cracking in eastern abutment looking south; (b) Abutment column cracking; (c) Cracking at top of pier; (d) Settlement of eastern approach looking west.

6.3.2 Mororimu Overbridge [-42.2166, 173.8686]

The Mororimu Overbridge is a 4-span reinforced concrete bridge also constructed in 1951 located about 100 m northwest along SH1 from the Mororimu Stream Bridge. The spans are supported on multi-column bents, with four columns for the outer piers and a two-column portal frame at the central pier to accommodate trains. All three piers are founded on strip footings. The Mororimu Overbridge is flat and straight (i.e., no tilt or curvature).

Cracking was observed at the top of the abutment and pier columns as shown in Figure 6.61(a) and (b). There was extensive cracking below the knee joints of the portal frame at the central pier, with the damage to the northern column shown in Figure 6.61(c). The damage at each pier was most severe at the top of the shortest column, with concrete spalling and some exposed reinforcement as shown in Figure 6.61(d). The geotechnical damage was similar to that observed at the Mororimu Stream bridge, with settlement in the approaches, settlement of the fill ahead of the abutments, and soil gapping around the base of the piers. No surficial evidence of liquefaction was observed at the Mororimu Overbridge site.

Figure 6.61: Structural damage observations at the Mororimu Overbridge [-42.2166, 173.8686]: (a) Abutment column cracking; (b) Damage to pier columns; (c) Cracking below knee joint of central pier column; (d) Exposed reinforcement at top of pier column.

6.3.3 Clarence River Bridge [-42.1592, 173.9103]

The Clarence River Bridge is a 6-span balanced cantilever, single cell box girder bridge built in 1975 and seismically retrofit in 2007. The superstructure is supported on wall piers, and is monolithic with the piers. The piers are supported by two concrete piles each, and the abutments are supported on steel H-piles. The box girder supporting the deck is seated at the abutments on three elastomeric bearings, and is anchored to the abutments by a row of hold-down rods to prevent uplift during live loading. The Clarence River Bridge is sloped vertically, with the north side higher than the south side, and is moderately curved in the horizontal direction, with the concave side to the east (Palermo et al., 2017).

The structural damage at the Clarence River Bridge was primarily confined to the substructure, and the damage patterns are indicative of primarily of transverse movement during shaking. As shown in Figure 6.62(a), cracking was observed where a vertical member providing transverse resistance to the deck frames into the abutment wall. This cracking is indicative of transverse deck movement during shaking. The hold-down rods tying the deck beams to the abutment seat display corresponding damage, with residual displacements evident in the transverse direction as shown in Figure 6.62(b). Settlement of the deck relative to the abutment seat was also evident as shown in Figure 6.62(c). Further evidence of transverse movement was observed at the pier footings, where as shown in Figure 6.62(d) and Figure 6.63(a), there was concrete spalling and cracking at the pier-footing interface and in the top surface of the footing.

Figure 6.62: Structural damage at Clarence River Bridge [-42.1592, 173.9103]: (a) Cracking in transverse abutment wall; (b) Residual deformation in hold down rod securing deck to abutment; (c) Deck settlement at abutment; (d) Concrete spalling at base of pier.

Figure 6.63: Damage at Clarence River Bridge [-42.1592, 173.9103]: (a) Cracking in top of footing; (b) Settlement of fill ahead of abutment; (c) Soil gapping at base of pier; (d) Spreading cracks in roadway at southern approach looking south.

Settlement was observed in both approaches, but the magnitude was limited by the presence of an approach slab. The settlement at the northern approach opened an approximately 25 mm wide gap between the abutment and slab. Settlement of the fill ahead of the abutment wall was also observed as shown in Figure 6.63(b), and soil gapping was noted at the base of several piers. Figure 6.63(c) shows a representative example of this gapping. Roadway cracks indicative of transverse approach spreading were observed on both sides of the bridge, and were particularly severe in the southern approach as shown in Figure 6.63(d).

6.3.4 Lyell Creek Bridge [-42.3892, 173.6773]

The bridge crossing Lyell Creek on Hawthorne Road is an east-west oriented single-span bridge with a total deck length of 7.15 m. The bridge crossing is slightly skewed relative to the river, making an angle of approximately 65 degrees to the river. The deck consists of wooden planking supported by two longitudinal I-beams. The I-beams appear to be tied together at two locations by U-sections. At both ends, the deck is supported on concrete abutments. This bridge was rendered unusable after the earthquake on account of the large movements of the abutments and deck slab. Figure 6.64 shows an overview of the Lyell Creek Bridge site.

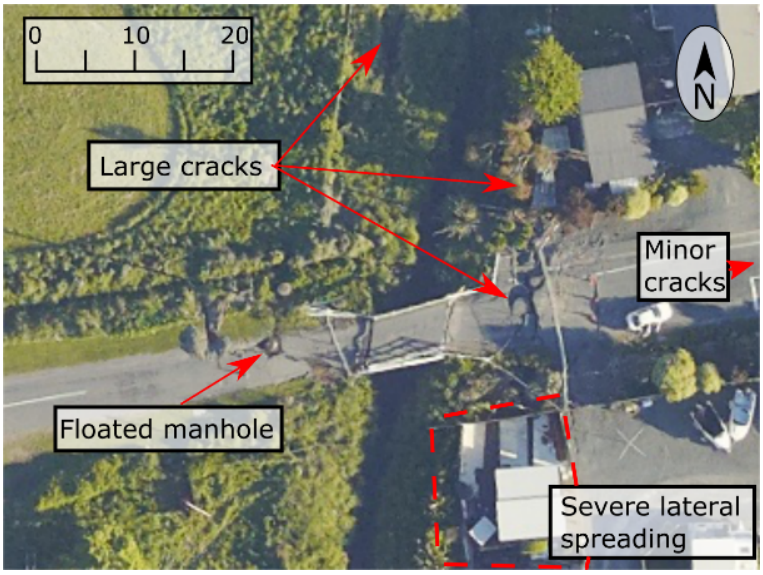

Figure 6.64: Site layout and features of interest at Lyell Creek Bridge [-42.3892, 173.6773].

On the eastern side of the bridge, cracks around 4 cm wide began on the south side of the road, (approximately 1.7 m from the end of the deck), running parallel to the road, becoming oriented at 45° to the road approximately 5 m from the end of the deck. This crack became approximately 20 cm wide at the centre of the road. One major crack 50 cm in width and parallel to the river was observed 9 m from the end of the deck. The crack to the east of the bridge was located a distance of 15.5 m from the end of the deck, was perpendicular to the road, and approximately 5 cm wide. The road appears to drop 15 cm to the river side of this crack. At the south of the road, the crack rotated 45° in plan and continued towards the river. Along the road, there were a number of cracks approximately 2 cm wide between 5 m and 19 m from the river. Figure 6.65(a) shows some of these features in the eastern approach.

Figure 6.65: Approach cracking at Lyell Creek Bridge [-42.3892, 173.6773]: (a) Eastern approach looking east; Note: crack at 9, from the bridge abutment (location of field member) was 50 cm wide, and had a vertical offset of 30 cm. (b) Western approach looking east.

Some earthwork had been carried out on the western side of the bridge as shown in Figure 6.65(b), and at the time of the visit, there were no obvious lateral spreading cracks crossing through the road to the west of the bridge. Heavy cracking was apparent around a manhole located on the north side of the road, 10 m west of the bridge abutment. Aerial photography taken on 14 November shows that there were three large cracks spreading out from the

manhole to the west, north (roughly parallel to the river), and to the southeast. At the time of the survey, the relative vertical offset between the manhole cover and the road surface was approximately 520 mm, of which a large part appears to be composed of settlement of the backfill. The lines of the cracks suggest that they could be associated with buried services. Close inspection of aerial photography shows that there were large lateral spreading cracks in the on the grassy banks both to the north and south of the bridge, though these were not observed on foot.

Figure 6.66: Back rotation of east and west abutments at Lyell Creek Bridge [-42.3892, 173.6773]: (a) Looking south at bridge; (b) Looking north at bridge.

Both the east and west abutments experienced large rotations, with the base of the abutment moving inwards toward the waterway as shown in Figure 6.66. At the northeast corner of the bridge, the deck slab and deck beam appear to have remained connected together, but have displaced approximately 630 mm northwards relative to their original anchor point on the abutment. As shown on the left side of Figure 6.67, to accommodate the lateral movement, the north deck beam was forced to override the lateral guide lug. The vertical displacement of the deck at the location of the deck-beam was 400 mm relative to the top of the abutment. In addition to these translational movements, the deck and beam have rotated 12° anticlockwise in plan. The deck beams appear to have been anchored to the abutment using single steel bars. The movement at this abutment has pulled the bar out of the abutment, and the lateral movement has created two 90° bends in the bars as shown in Figure 6.68(b).

Figure 6.67: Eastern side of Lyell Creek Bridge [-42.3892, 173.6773]. Photo facing west.

Figure 6.68: Damage at Lyell Creek Bridge [-42.3892, 173.6773]: (a) Eastern end of bridge looking north; (b) Bent anchor bars at east abutment-deck connection; (c) Gap between deck and west abutment looking south; (d) Twisting of deck beams.

At the southeast corner of the bridge, the deck slab has separated from the deck beam and overridden the abutment, resulting in a vertical offset of 200 mm between the top of the deck slab and the abutment as shown on the right side of Figure 6.67 and in Figure 6.68(a). The deck slab appears to have translated northwards approximately 600 mm. The position of the deck beam relative to the abutment at the southeast corner was not inspected, but is assumed to have displaced northwards by around 600 mm (similar to the deck beam at the northeast corner). A large shear crack is present in the abutment where the southern deck beam meets the east abutment. Additional cracks outboard of the deck beam are also apparent on the eastern abutment.

On the west side of the bridge, the abutment has rotated such that the base moved inwards toward the river. Additionally, as shown in Figure 6.68(c), a gap has opened consistent with the rotation (in plan) of the deck slab observed at the east end of the bridge. The southern deck beam translated laterally to the south by 100 mm, where it was restrained by the lateral guide lug. As a result of the abutment rotation, the base of the southern deck beam is in contact with the western abutment, while there is a 180-200 mm horizontal gap between the top of the beam and the abutment. It is estimated that the rotation of the abutment in the vertical plane is around 16°. At the northwest corner, the bottom of the deck beam has remained in contact with the abutment, however, the rotation of the deck slab has bent the end flange plate at the top of the deck beam and twisted the deck beam structure as shown in Figure 6.68(d). The deck beam does not appear to have translated in plan relative to the abutment.

6.3.5 Other Bridges and Culverts in Kaikoura Township

6.3.5.1 Middle Creek Railway Bridge

The railway crosses Middle Creek just southwest of the oxidation ponds at the location marked on Figure 4.126. The concrete bridge deck is supported by two piers which are supported by 4 × 2 pile groups (Figure 6.69). As shown in Figure 6.70, ejected material was observed on the east side of the bridge, close to the north pier and abutment. The settlement of the approach fills left the railway unsupported at both ends of the bridge as shown in Figure 6.71, while Figure 6.72 captures the failure in the concrete abutment at the north end of the bridge due to the passive soil loads.

Figure 6.69: Middle Creek Railway Bridge (facing northwest) [-42.3672, 173.6862].

Figure 6.70: Liquefaction close to the north pier and abutment of Middle Creek Railway Bridge (facing southeast) [-42.3670, 173.6861].

(a)

(b)

Figure 6.71: View along the tracks of Middle Creek Railway Bridge. Settlement of the approaches to the bridge left the rails unsupported: (a) Looking north [-42.3672, 173.6860]; (b) View looking south [-42.3670, 173.6861].

Figure 6.72: Damage to the north abutment of the Middle Creek Railway Bridge facing northwest [-42.3670, 173.6861].

6.3.5.2 Middle Creek Bridge – Mt Fyffe Rd

An ~9.5-m long, single lane bridge that crosses Middle Creek on Mt Fyffe Road also experienced damage, as shown in Figure 6.73 through Figure 6.76. As shown in Figure 6.73(b), fill was placed to compensate for subsidence of the both the north and south approaches and the barriers on the northern approach rotated outward. Also, both the reinforced concrete north and south abutments to the bridge experienced cracking (Figure 6.74-Figure 6.76).

(a) (b)

Figure 6.73: Bridge crossing Middle Creek on Mt Fyffe Road (8 Dec 2016): (a) Cracking of concrete on south abutment (facing southwest) [-42.3692, 173.6548]; (b) Outward rotation of barriers on approach (facing south) [-42.3691, 173.6547].

Figure 6.74: Damage to the south abutment on the east side of the bridge (8 Dec 2016, facing south) [-42.3692, 173.6547].

Figure 6.75: Damage to the north abutment on the east side of the bridge (8 Dec 2016, facing north) [-42.3692, 173.6549].

Figure 6.76: Damage to the north abutment on the west side of the bridge (8 Dec 2016, facing north) [-42.3692, 173.6547].

6.3.5.3 Culverts

Lateral spreading was observed in the area of the Waimagarara culvert on State Highway 1 (Athelney Road). To the north of the culvert, lateral spreading cracks were parallel to the road, with the spreading occurring towards small drainage ditches. Lateral spreading displacements on the east side of the road, north of the culvert, were of the order of 30-50 cm wide and typically 60 cm deep. These cracks were offset from the road, by approximately 2 m (Figure 6.77 and Figure 6.78). Cracks in the road and ejecta on the south side of the Waimagarara culvert are shown in Figure 6.79 and Figure 6.80. Damage was also noted on culverts located on the smaller roads west of Kaikoura on Hawthorne Road (Figure 6.81) and Mill Road (Figure 6.82), often with cracking in the wingwalls.

Figure 6.77: Lateral spreading cracks at the side of Athelney Road (9 Dec 2016, facing north) [-42.3598, 173.6765]. Note the drainage ditch to the right of the photo.

Figure 6.78: Cracking on the north-side of the Waimagarara culvert on Athelney Road (9 Dec 2016, facing south) [-42.3599, 173.6765].

Figure 6.79: Cracking on the south side of the Waimagarara culvert on Athelney Road (9 Dec 2016, facing north) [-42.3606, 173.6765].

(a)

(b)

Figure 6.80: Ejecta on the south of Waimagarara Culvert on Athelney Road, approximately 10 m from the creek (9 Dec 2016): (a) East side of the road facing east [-42.3603, 173.6766]; (b) West side of the road facing north [-42.3603, E173.6765].

Figure 6.81: Cracking in the concrete at Hawthorne Road culvert (8 Dec 2016, facing northwest) [-42.3900, 173.6675].

Figure 6.82: Failure of the northwest wingwall of the Lyell Creek culvert on Mill Road (8 Dec 2016, facing west) [-42.3765, 173.6788].

6.3.6 Oaro Overbridge [-42.5121, 173.5063]

The Oaro Overbridge is a 5-span reinforced concrete bridge spanning railroad tracks on SH1 just north of Oaro. The middle piers (adjacent to railroad tracks) are single-column hammerhead bents, and the outer piers are four-column bents. It appears that the superstructure is integral to the piers and abutments at either end (unconfirmed). The Oaro Overbridge is curved, with the concave side to the west, and tilted such that the eastern side is higher than the western side. Significant settlement of at least 1.0 m was observed at the southern approach as shown in Figure 6.83. This settlement was slightly larger on the eastern side and large spreading cracks are apparent throughout the approach roadway. It appears that the approach fill has spread primarily towards the west (to the left in Figure 6.83). Direct photographic evidence is not currently available for the northern side, but it is apparent from the bent guardrails on the far side of the bridge in Figure 6.83(a) that some settlement occurred there as well. No surficial evidence of liquefaction or cracking consistent with spreading in the longitudinal direction was reported at the Oaro Overbridge site, but at the time of reporting only rapid reconnaissance results were available for this location.

Figure 6.83: Settlement and severe approach roadway cracking at southern abutment to Oaro Overbridge [-42.5121, 173.5063] looking north. Photos by D. Dizhur and M. Giaretton.

The observed structural damage was primarily to the bridge substructure, and was particularly concentrated in the abutments and the pier columns closest to the abutments. At the southern end, shown in Figure 6.84(a), moderate flexural cracking was observed at the top of all four pier columns just below the knee of the joint with the superstructure. Figure 6.84(a) also shows the settlement of the fill ahead of the south abutment, resulting in exposed piles. Based on the markings evidenced on the abutment wall, this fill has subsided at least 50 cm. Figure 6.84(b) shows a corresponding view of the northern end of the bridge. On this side, the damage at the top of the pier columns was much more severe, with concrete spalling, significant cracks passing all the way through the columns, and exposure of longitudinal reinforcement. Figure 6.84(c) provides a closer view of the tops of the two westernmost columns of the northern pier. Figure 6.84(b) also shows the more moderate flexural cracks near the base of the pier columns on the northern end. The slope ahead of the northern abutment is much less abrupt than at the south side, and settlements in this area appear to be less than observed on the southern end. A severe crack was observed over the entire length of the north abutment wall as shown in Figure 6.84(d). This crack is just below where the beams connect to the abutment, and the attendant spalling and bent reinforcing steel are indicative of significant pounding at this end.

Figure 6.84: Damage at Oaro Overbridge [-42.5121, 173.5063]: (a) Settlement of fill ahead of southern abutment and cracking at top of pier columns looking south; (b) Cracking in fill ahead of northern abutment and plastic hinging at top of pier columns looking north; (c) Closer view of damage at top of pier columns in northernmost pier looking north; (d) Cracking across face of northern abutment wall, just below deck beams looking north. Photos courtesy of D. Dizhur and M. Giaretton.

The central hammerhead piers were much less damaged than the four-column piers closer to the abutments. As shown in Figure 6.85(a), these piers are both longer and more substantial than those nearer the ends. Some relatively minor cracking in the horizontal member just below the deck beams was observed in the eastern side of the northern face of the northern hammerhead pier (upper left in Figure 6.85(a)). Minor flexural cracking was also observed at the base of this pier column as shown in Figure 6.85(b).

Figure 6.85: Damage at Oaro Overbridge [-42.512089, 173.506345]: (a) Northernmost central hammerhead pier looking south; (b) Flexural cracking at base of northernmost hammerhead pier. Photos courtesy of D. Dizhur and M. Giaretton.

6.3.7 Oaro River Rail Bridge [-42.514025, 173.50682]

Significant damage was observed at a railroad bridge crossing the Oaro river about 100 m due south of the Oaro Overbridge. This is an 8-span reinforced concrete bridge with integral wall piers and abutments located less than 30 m from the ocean. Significant residual lateral deformation was observed at this bridge, resulting in the bent rails shown in Figure 6.86(a). It appears that the bridge has rotated as a rigid body such that the northern end has moved eastwards by about 25-50 cm while the southern end has stayed essentially in place. No cracks are evident in the northern approach as would be expected for movement of the fill material, supporting the hypothesis of structural movement. Figure 6.86(b) indicates that regardless of the source of the movement, the entire bridge structure has remained intact. Settlement of the approach fill was also evident at both sides of the bridge.

Figure 6.86: Damage at Oaro River Rail Bridge [-42.514025, 173.50682]: (a) Residual lateral deformation towards the east at the northern abutment has bent the tracks (photo looking south); (b) Northern abutment looking north. Photos courtesy of D. Dizhur and M. Giaretton.

6.3.8 Bridge on Clarence Valley Road [-42.11066, 173.84156]

The bridge crossing the Clarence River on the Clarence Valley Road in an area of surface faulting and severe flooding experienced complete collapse. This bridge is located approximately 10 km west from SH1 northwest of Clarence and Waipapa Bay, and in contrast to some of the rural bridges discussed from the Hurunui District in earlier sections of this report, the Clarence Valley Road Bridge was a relatively newly built structure spanning a reasonably significant distance. Figure 6.87 shows a view of the collapsed bridge site from the western side of the Clarence River taken at some point in the week following the 14 November. As shown, the superstructure of the bridge has completely collapsed. Severe surface faulting was present in this area in addition to the flooding shown in Figure 6.87.

Figure 6.87: Collapse of Clarence Valley Road Bridge [-42.11066, 173.84156]. Photo taken from western side looking east (stuff.co.nz, 2016).

References

Dizhur, D. and Giaretton, M. (2016). Personal communication. November 2016.

Palermo, A., Liu, R., Rais, A., McHaffie, B., Andisheh, K., Pampanin, S., Gentile, R., Nuzzo, I., Granerio, M., Loporcaro, G., McGann, C.R. and Wotherspoon, L.M. (2017). "Performance of road bridges during the 14 November 2016 Kaikōura earthquake". *Bulletin of the New Zealand Society for Earthquake Engineering*, **50**(2): 253-270.

stuff.co.nz (2016) Quake shuts off Clarence Valley access, isolates farmers and residents. http://www.stuff.co.nz/business/farming/86674297/Quake-shuts-off-Clarence-Valley-access-isolates-farmers-and-residents. Last accessed 08 June 2017.